Surface modes on nanostructured metallic surfaces

S. Collin,[1,*] C. Sauvan,[1,2] C. Billaudeau,[1] F. Pardo,[1] J. C. Rodier,[2] J. L. Pelouard,[1] and P. Lalanne[2]
[1]*Laboratoire de Photonique et de Nanostructures (LPN-CNRS), Route de Nozay, 91460 Marcoussis, France*
[2]*Laboratoire Charles Fabry de l'Institut d'Optique, CNRS, Univ. Paris-Sud, Campus Polytechnique, RD128, 91127 Palaiseau, France*
(Received 23 December 2008; published 6 April 2009)

The dispersion properties of surface modes supported by metal/dielectric interfaces perforated by two-dimensional arrays of subwavelength apertures are studied. An analytical surface-impedance model is derived. It provides closed-form expressions for the dispersion relation of surface modes and allows to take into account the aperture geometry and the dispersive and dissipative properties of the metal. The model predicts the dispersion relation and the mode lifetime, in quantitative agreement with fully vectorial computational results and with experimental data obtained at optical frequencies. The analysis reveals a double plasmonic band gap in the center of the Brillouin zone for a square array. It additionally clarifies the effects of various different geometrical and material parameters on the surface properties.

DOI: 10.1103/PhysRevB.79.165405 PACS number(s): 42.25.Bs, 42.70.Qs, 73.20.Mf, 78.68.+m

I. INTRODUCTION

In recent years, there has been much interest in controlling light-matter interactions by introducing structures on length scales equal to or smaller than the wavelength of the light. By varying the shape and the size of the inclusions, it is possible to control the effective refractive index and thus to add new possibilities to the range of materials available in optics (see Refs. 1–3, for instance). Like other optical waves, the properties of surface-plasmon polaritons (SPPs) can be tailored by engineering the respective contributions of the photonic and the electronic parts of the mode. This can be achieved by puncturing the metallic surface with arrays of subwavelength apertures. Such textured interfaces are known to strongly alter the radiative and nonradiative dampings of SPPs (Refs. 4 and 5) to allow strong light confinement regimes[6] or to create a new family of bounded modes for interfaces with very large metal conductivities.[7–9]

Despite their importance and while much effort has been devoted to the characterization of their optical properties, there has been little theoretical work on surface modes supported by periodically textured interfaces. A microscopic model based on the scattering of SPPs has been recently derived.[10] Although it provides a clear foundation for the existence of the mode, it relies on fully vectorial calculations that prevent full analiticity. Some analytical investigations have been conducted but only for perfectly conducting screens and for asymptotic situations (hole array with period much smaller than the wavelength).[8,9,11,12] Finally, numerical studies have been performed at optical frequencies with fully vectorial computations.[13] Although the latter treatment is virtually exact at all frequencies and allows a quantitative agreement with experiments, it is rather computationally demanding and lacks from sufficient physical insight. As a consequence, one usually uses the analytical expression of the flat-interface SPP for the design or the interpretation of experimental results. Unfortunately, this drastic approximation results in systematic frequency deviations with experimental observations and in the impossibility of taking into account the impact of the aperture geometry.[14–18]

In this paper, we present a formalism that yields explicit formulae for the energy and the lifetime of surface modes supported by textured interfaces. The formalism developed in Sec. II is based on the definition of a specific periodic surface impedance for the textured metal. It leads to a simple analytical treatment. The surface mode dispersion relation is determined by a 3×3 matrix whose coefficients are given by closed-form expressions. In these expressions, the aperture geometry and the metal conductivity appear explicitly, thus allowing a simple understanding and engineering of the optical properties of textured metallic surfaces. In Sec. III, the model is used to finely analyze the band structure of a metallic square array. Comparisons with fully vectorial computational results evidence that the 3×3 matrix treatment is able to accurately predict the complex dispersion relation of the surface modes with the lowest energies. Deviations are only observed for high-energy bands. Section IV discusses the influence on the surface properties of various parameters such as the metal conductivity, the aperture area, and the aperture shape. Comparisons with experimental results further validate the model. In addition to its simplicity that may be useful for further engineering textured metallic surfaces, the analytical treatment allows for an in-depth understanding of all the various physical and geometrical parameters that govern the plasmonic properties of periodically textured surfaces.

II. SURFACE-IMPEDANCE MODEL

We consider an interface between two semi-infinite regions (I) and (II) (see Fig. 1). All materials are nonmagnetic.

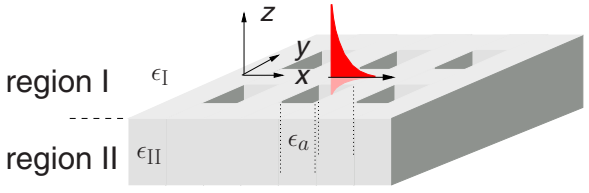

FIG. 1. (Color online) Interface between a dielectric half space (region I) and a metallic substrate perforated by a lattice of semi-infinite apertures (region II). The propagation of SPP modes in the x direction is schematically represented in red.

Region (I) is a homogeneous dielectric medium (permittivity ϵ_{I}). Region (II) is composed of a metallic medium (permittivity ϵ_{II}) drilled with a rectangular array (periods d_x and d_y) of subwavelength apertures that are filled with a dielectric material (permittivity ϵ_a). The apertures fill factor is denoted by α. We restrict ourselves to surface modes with $k_y=0$.

Let us first briefly consider the case of a flat interface $\alpha=0$. In every uniform region, the electromagnetic field is a plane wave with a complex wave vector $\mathbf{k}_i=k_x\mathbf{u_x}+k_{zi}\mathbf{u_z}$, $i=\mathrm{I},\mathrm{II}$. The SPP mode propagating along the surface exists only in TM polarization ($H_z=0$). Its dispersion relation can be obtained by writing the continuity of the tangential fields across the interface, $\mathbf{E_{tI}}=\mathbf{E_{tII}}$ and $\mathbf{H_{tI}}=\mathbf{H_{tII}}$. We can introduce in these continuity relations the surface impedance Z_i of each uniform half space defined by[19]

$$\mathbf{E_{t}}_i = Z_i \mathbf{n}_i \times \mathbf{H_{t}}_i, \tag{1}$$

where $\mathbf{n}_i$ is a unit vector normal to the interface ($\mathbf{n}_{\mathrm{I}}=-\mathbf{u}_z$ and $\mathbf{n}_{\mathrm{II}}=\mathbf{u}_z$) and $Z_i=k_{zi}/\omega\epsilon_0\epsilon_i$. Finally, the dispersion relation of the flat-interface SPP is simply given by[4]

$$Z_{\mathrm{I}} + Z_{\mathrm{II}} = 0. \tag{2}$$

Hereafter, we generalize this well-known expression for surface modes supported by periodically textured interfaces. The key point is to define a surface impedance for the metallic region perforated by periodic apertures.

A. Surface impedance of the uniform dielectric region

To derive the dispersion relation of the surface modes supported by the periodic interface in Fig. 1, we follow the same method as for the flat surface and write the continuity of $\mathbf{E_t}$ and $\mathbf{H_t}$ across the interface. Therefore, in the following, we only consider the expressions of the tangential fields. Moreover, like in the flat-interface case, only TM-polarized plane waves ($H_z=0$) are considered in the following description.

In the uniform half space defined by region (I), the electromagnetic field can be rigorously written as a Rayleigh expansion,[13]

$$\mathbf{E_{tI}}(x,y,z) = \sum_{n,p} \mathbf{E_{tI}}^{(n,p)} e^{i(k_x^{(n)}x + k_y^{(p)}y + k_{z\mathrm{I}}^{(n,p)}z)}, \tag{3a}$$

$$\mathbf{H_{tI}}(x,y,z) = \sum_{n,p} \mathbf{H_{tI}}^{(n,p)} e^{i(k_x^{(n)}x + k_y^{(p)}y + k_{z\mathrm{I}}^{(n,p)}z)}. \tag{3b}$$

Equations (3a) and (3b) are discrete sums of plane waves where $k_x^{(n)}=k_x+n2\pi/d_x$, $k_y^{(p)}=p2\pi/d_y$, and $k_x^{(n)2}+k_y^{(p)2}+k_{z\mathrm{I}}^{(n,p)2}=\epsilon_{\mathrm{I}}k_0^2$, with $k_0=2\pi/\lambda$. Without any approximation, one may associate a surface impedance to every plane wave (n,p),

$$\mathbf{E_{tI}}^{(n,p)} = -Z_{\mathrm{I}}^{(n,p)} \mathbf{u}_z \times \mathbf{H_{tI}}^{(n,p)}, \tag{4}$$

where $Z_{\mathrm{I}}^{(n,p)}=k_{z\mathrm{I}}^{(n,p)}/\omega\epsilon_0\epsilon_{\mathrm{I}}$.

B. Surface impedance of the nanostructured metallic region

In the periodically textured half space [region (II)], the electromagnetic field can be rigorously written as a Bloch-mode expansion.[13] However, some approximations are necessary to be able to define a surface impedance for the textured metal. They all rely on the opacity of the metal and on the small aperture size compared to the wavelength and the period.

(1) In the apertures, we use a single-mode approximation. The field is described by the guided mode of an isolated hole, and we assume that a surface impedance Z_a can be introduced by using the definition of the impedance for a perfect metal waveguide provided that the calculation of the propagation constant κ is performed by using the real metal permittivity with a finite conductivity. The hole mode, in general the fundamental evanescent one, is selected according to symmetry considerations, as will be discussed later.

(2) In the metal, we assume that the solution in the limit of infinitely small apertures remains valid. The field is then given by a Rayleigh expansion similar to Eq. (3), and a surface impedance $Z_m^{(n,p)}$ can be introduced for every plane wave (n,p).

The single-mode approximation and the continuity of $\mathbf{H_t}$ at $z=0$ allow us to write the tangential electric field in the apertures as

$$\mathbf{E}_{\mathrm{tII}}^{\mathrm{ap}}(x,y,0) = \sum_{n,p} Z_a \mathbf{u}_z \times \mathbf{H_{tI}}^{(n,p)} e^{i(k_x^{(n)}x + k_y^{(p)}y)}. \tag{5}$$

In the limit of infinitely small apertures, the field in the metal is given by a discrete sum of plane waves

$$\mathbf{E}_{\mathrm{tII}}^{\mathrm{met}}(x,y,z) = \sum_{n,p} \mathbf{A}^{(n,p)} e^{i(k_x^{(n)}x + k_y^{(p)}y - k_{z\mathrm{II}}^{(n,p)}z)}, \tag{6a}$$

$$\mathbf{H}_{\mathrm{tII}}^{\mathrm{met}}(x,y,z) = \sum_{n,p} \mathbf{B}^{(n,p)} e^{i(k_x^{(n)}x + k_y^{(p)}y - k_{z\mathrm{II}}^{(n,p)}z)}, \tag{6b}$$

where $k_x^{(n)2}+k_y^{(p)2}+k_{z\mathrm{II}}^{(n,p)2}=\epsilon_{\mathrm{II}}k_0^2$. Moreover, the continuity of the tangential field implies that $\mathbf{A}^{(n,p)}=\mathbf{E_{tI}}^{(n,p)}$ and $\mathbf{B}^{(n,p)}=\mathbf{H_{tI}}^{(n,p)}$. Like in region (I), one may associate a surface impedance $Z_m^{(n,p)}=k_{z\mathrm{II}}^{(n,p)}/\omega\epsilon_0\epsilon_{\mathrm{II}}$ with every plane wave (n,p), and finally the tangential electric field in the metal can be written as

$$\mathbf{E}_{\mathrm{tII}}^{\mathrm{met}}(x,y,0) = \sum_{n,p} Z_m^{(n,p)} \mathbf{u}_z \times \mathbf{H_{tI}}^{(n,p)} e^{i(k_x^{(n)}x + k_y^{(p)}y)}. \tag{7}$$

Equations (5) and (7) can be straightforwardly rewritten as a single expression that defines a *periodic surface impedance* for the textured region (II),

$$\mathbf{E}_{\mathrm{tII}}(x,y,0) = \sum_{n,p} Z_{\mathrm{II}}^{(n,p)}(x,y) \mathbf{u}_z \times \mathbf{H_{tI}}^{(n,p)} e^{i(k_x^{(n)}x + k_y^{(p)}y)}, \tag{8}$$

with

$$Z_{\mathrm{II}}^{(n,p)}(x,y) = \begin{cases} Z_a = \mu_0\omega/\kappa & \text{in the holes} \\ Z_m^{(n,p)} = k_{z\mathrm{II}}^{(n,p)}/\omega\epsilon_0\epsilon_{\mathrm{II}} & \text{in the metal.} \end{cases} \tag{9}$$

In Eq. (9), $Z_m^{(n,p)}$ is the impedance of the plane wave (n,p) in the metal and Z_a is the impedance of the hole mode. The latter is chosen among the less attenuated modes of the metallic waveguide (in general the fundamental evanescent mode), which appear to be TE polarized. For TE-guided modes, $Z_a=\mu_0\omega/\kappa$ where κ is the propagation constant of

the mode. The selection rules for the guided mode also include some symmetry considerations, as will be discussed later.

By taking advantage of the periodicity of $Z_{\mathrm{II}}^{(n,p)}(x,y)$ in Eq. (8), we can write the continuity of $\mathbf{E_t}$ in the Fourier space, which leads to the following relation between the Fourier components of the electric and magnetic fields:

$$\mathbf{E}_{\mathrm{tI}}^{(n,p)} = \sum_{q,l} Z_{n-q,p-l}^{(q,l)} \mathbf{u}_z \times \mathbf{H}_{\mathrm{tI}}^{(q,l)}, \tag{10}$$

where $Z_{n-q,p-l}^{(q,l)}$ are the Fourier coefficients of the periodic surface impedance $Z_{\mathrm{II}}^{(q,l)}(x,y)$.

Let us emphasize that, in contrast to previous approaches,[8] the use of a specific periodic impedance for the perforated metal allows us to take into account the effect of the finite conductivity of the metal. Moreover, Eq. (10) shows that the Fourier components of the field are coupled together through the Fourier coefficients of the impedance. A similar result is classically obtained in periodic dielectric media, such as photonic crystals, where the Fourier components of the field are coupled together through the Fourier coefficients of the permittivity.[20] Equation (10) evidences that within the model approximations, the descriptions of the Bloch modes propagating in a photonic crystal and of those supported by a perforated metallic surface are conceptually identical; the periodic permittivity being simply replaced by a periodic surface impedance. Evidencing this analogy is an important result of the model.

C. Dispersion matrix

With the expressions of the surface impedance in regions (I) and (II) given by Eqs. (4) and (10), the continuity relation can be written as

$$\forall (n,p), \sum_{q,l} (Z_{\mathrm{I}}^{(n,p)} \delta_{n-q,p-l} + Z_{n-q,p-l}^{(q,l)}) \mathbf{u}_z \times \mathbf{H}_{\mathrm{tI}}^{(q,l)} = 0. \tag{11}$$

In this matrix equation $D \cdot (\mathbf{u}_z \times \mathbf{H_t}) = 0$, the size of the dispersion matrix D depends on the number of plane waves considered in the Rayleigh expansions. The surface modes are the complex-frequencies solutions of $\det(D)=0$ calculated for real values of k_x in the first Brillouin zone. The nondiagonal terms of D [line (n,p), column (q,l)] are given by the Fourier coefficients $Z_{n-q,p-l}^{(q,l)}$ of the periodic surface impedance of the textured metal. The diagonal terms of D are equal to $Z_{\mathrm{I}}^{(n,p)} + \langle Z_{\mathrm{II}}^{(n,p)} \rangle$, where $\langle Z_{\mathrm{II}}^{(n,p)} \rangle = Z_{00}^{(n,p)} = \alpha Z_a + (1-\alpha) Z_m^{(n,p)}$ is the average surface impedance of the textured metal.

The matrix coefficients clearly evidence the physical nature of the surface modes supported by a textured metallic interface. The diagonal terms characterize an effective surface mode that propagates on an effective flat interface with an impedance equal to the average impedance $\langle Z_{\mathrm{II}}^{(n,p)} \rangle$. Its value is driven by the metal conductivity and the aperture shape and size as will be discussed in Sec. IV. The dispersion relation of this effective mode is folded inside the first Brillouin zone because of the periodic nature of the surface; each folded branch corresponding to a plane wave (n,p) in the Rayleigh expansion [see Eq. (3)]. Moreover, because of the nondiagonal terms, the different folded branches corresponding to the average impedance contribution are coupled together through the higher-order Fourier coefficients of the periodic impedance $Z_{n-q,p-l}^{(q,l)}$. These Fourier coefficients represent the coupling strength between the waves (n,p) and (q,l) introduced by the nanostructuration. Intuitively, this coupling that additionally brings radiative damping into play will be important only for k_x values corresponding to the crossing of several folded branches and it will mainly involve the plane waves associated with this crossing.

In the following, we restrict ourselves to the surface modes with the lowest frequencies and we neglect the coupling between the x and y directions. The matrix D then splits into two independent 3×3 submatrices and, as we shall see, only three plane waves are sufficient to accurately describe the surface mode; these waves are labeled by $(n,p)=\{(-1,0),(0,0),(+1,0)\}$ and $(n,p)=\{(0,-1),(0,0),(0,+1)\}$. Let us emphasize that by including the propagating zero order, which represents the coupling to far-field radiation, the treatment accounts for the total losses (radiative and nonradiative) of the surface modes. The 3×3 matrix describing the dispersion relations of the surface modes associated with the $(\pm 1,0)$ plane waves is given by

$$\begin{pmatrix} Z_{\mathrm{I}}^{(-1,0)} + \langle Z_{\mathrm{II}}^{(-1,0)} \rangle & Z_{-10}^{(0,0)} & Z_{-20}^{(1,0)} \\ Z_{10}^{(-1,0)} & Z_{\mathrm{I}}^{(0,0)} + \langle Z_{\mathrm{II}}^{(0,0)} \rangle & Z_{-10}^{(1,0)} \\ Z_{20}^{(-1,0)} & Z_{10}^{(0,0)} & Z_{\mathrm{I}}^{(1,0)} + \langle Z_{\mathrm{II}}^{(1,0)} \rangle \end{pmatrix}. \tag{12}$$

A similar matrix describes the dispersion relations of the surface modes associated with the $(0, \pm 1)$ waves,

$$\begin{pmatrix} Z_{\mathrm{I}}^{(0,-1)} + \langle Z_{\mathrm{II}}^{(0,-1)} \rangle & Z_{0-1}^{(0,0)} & Z_{0-2}^{(0,1)} \\ Z_{01}^{(0,-1)} & Z_{\mathrm{I}}^{(0,0)} + \langle Z_{\mathrm{II}}^{(0,0)} \rangle & Z_{0-1}^{(0,1)} \\ Z_{02}^{(0,-1)} & Z_{01}^{(0,0)} & Z_{\mathrm{I}}^{(0,1)} + \langle Z_{\mathrm{II}}^{(0,1)} \rangle \end{pmatrix}. \tag{13}$$

These expressions of the dispersion matrix are valid for any aperture shape. In the following, we restrict ourselves to rectangular apertures of width w_x and w_y. In this case, the Fourier coefficients of the periodic surface impedance $Z_{\mathrm{II}}^{(n,p)}(x,y)$ are given by

$$Z_{00}^{(n,p)} = \langle Z_{\mathrm{II}}^{(n,p)} \rangle = \alpha Z_a + (1-\alpha) Z_m^{(n,p)}, \tag{14a}$$

$$Z_{ql}^{(n,p)} = \alpha (Z_a - Z_m^{(n,p)}) \mathrm{sinc}\left(q\pi \frac{w_x}{d_x} \right) \mathrm{sinc}\left(l\pi \frac{w_y}{d_y} \right), \tag{14b}$$

where $\alpha = w_x w_y / d_x d_y$ is the apertures fill factor and $\mathrm{sinc}(x) = \sin(x)/x$. These coefficients obey the following symmetry properties: $Z_{ql}^{(n,p)} = Z_{-ql}^{(n,p)} = Z_{q-l}^{(n,p)} = Z_{-q-l}^{(n,p)}$. Moreover, an analytical expression of the propagation constant κ of the hole mode can be obtained as a function of the optogeometrical parameters ϵ_{II}, ϵ_a, w_x, and w_y.[21]

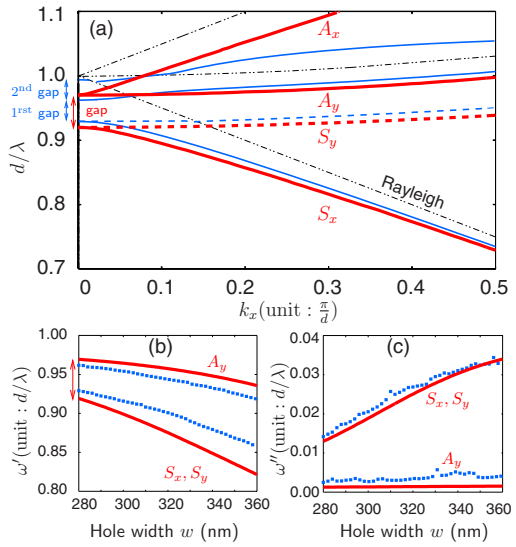

FIG. 2. (Color online) Model validation for a silver/air interface perforated by a 2D square array of square holes. (a) Dispersion diagram (width w=280 nm, period d=750 nm, and $\epsilon_1=\epsilon_a=1$). Thick red curves: analytical model predictions. Each curve is calculated with a single TE_{xx} waveguide mode in the apertures as follows: (S_x,TE_{01}), (S_y,TE_{10}), (A_x,TE_{11}), and (A_y,TE_{11}). Thin blue curves: results obtained with the fully vectorial modal method (Ref. 13). Dashed black lines: Rayleigh anomalies (grazing incidence condition for each diffracted wave). The surface modes can be excited by either TM polarized (solid curves) or TE-polarized (dashed curve) incident plane waves [see the discussion in Sec. III D]. (b) Real and (c) imaginary parts of the complex frequency $\omega=\omega'+i\omega''$ for the S_x, S_y and A_y modes as a function of the hole width for k_x=0. Model predictions (solid red curves) are compared to Fourier calculations (blue dots).

III. SURFACE MODES OF A SQUARE ARRAY

In this section, we analyze the band structure of a silver/air interface perforated by a square array of square holes of width w=280 nm and period $d_x=d_y=d$=750 nm. The permittivity of silver is taken from Ref. 22 and $\epsilon_1=\epsilon_a=1$. The model predictions for this interface are validated by comparison with the results of a three-dimensional (3D) fully vectorial calculation performed with the Fourier modal method.[13] We first discuss the dispersion diagram and the lifetime of the surface modes supported by this square array. Then we interpret an unexpected feature in the dispersion diagram evidenced by fully vectorial computations, namely, the appearance of a double plasmonic band gap. Finally, we link the model predictions to experimental results by discussing the free-space coupling of surface modes.

A. Dispersion diagram

The dispersion curves of the surface modes predicted by the 3×3 matrix treatment are shown in Fig. 2(a) with thick red curves. There are four branches associated with $(\pm1,0)$ and $(0,\pm1)$ plane waves. In this square lattice structure, these four modes are coupled together in the center of the Brillouin zone. Within the model, the coupling between $(\pm1,0)$ waves is treated independently of the coupling between $(0,\pm1)$ waves. The surface modes associated with the $(\pm1,0)$ waves correspond to the lower and upper modes in Fig. 2(a) (curves labeled S_x and A_x). They are mainly SPPs propagating in the x direction along an effective flat interface with an average impedance $\langle Z_{II}^{(-1,0)}\rangle$ and $\langle Z_{II}^{(1,0)}\rangle$, respectively. For k_x=0, these two counter-propagating modes couple together through the $Z_{20}^{(-1,0)}$ and $Z_{-20}^{(1,0)}$ Fourier coefficients of the impedance [see Eq. (12)]. The coupling results in the appearance of a band gap between symmetric (low-frequency mode S_x) and antisymmetric (high-frequency mode A_x) standing waves, like in one-dimensional (1D) structures.[23] A similar analysis can be made for the two other surface modes associated with $(0,\pm1)$ waves and labeled S_y and A_y, and—since the holes and the unit cell are square—there is a single band gap for k_x=0 between two modes with a double degeneracy. To take into account the symmetry difference of the surface modes for k_x=0, the S_x (respectively, S_y) branch in Fig. 2(a) is calculated with the fundamental symmetric TE_{01} waveguide mode of the apertures (respectively, TE_{10}) and the A_x and A_y branches are calculated with the antisymmetric hole mode with the lowest in-plane momentum: TE_{11}.

The dispersion curves have also been calculated with a 3D fully vectorial treatment (Fourier modal method) using ±15 Fourier harmonics in x and y directions [blue curves in Fig. 2(a)]. The results of the analytical model are in very good agreement with the vectorial Fourier calculations for the three lowest bands S_x, S_y (symmetric modes), and A_y (antisymmetric mode).

B. Mode lifetime

Figures 2(b) and 2(c) further validate the model predictions for the complex frequency $\omega'+i\omega''$ of the S_x, S_y, and A_y surface modes as a function of the hole width w. A good agreement between the surface-impedance model (red curves) and fully vectorial calculations (blue points) is demonstrated for hole widths up to nearly $d/2$. It is worth emphasizing that the total lifetime of the surface modes given by the imaginary part ω'' is accurately predicted by the 3×3 dispersion matrix, even for large holes that induce strong radiation losses.

Figure 2(c) shows very low and almost constant damping for the antisymmetric mode A_y, due to the absence of radiative coupling for k_x=0. On the contrary, radiation losses through the propagating (0,0) plane wave are predominant for the S_x and S_y modes, and the aperture widening induces a strong increase in the losses.

C. Second plasmonic band gap

The model predictions are found to be inaccurate for the upper branch A_x in the center of the first Brillouin zone and also for larger k_x values [see Fig. 2(a)]. For k_x=0, the fully vectorial calculations reveal the appearance of a second band gap between the A_x and A_y modes. This result shows that in a two-dimensional (2D) array, the x and y directions shall not be treated independently because of the weak coupling between the $(\pm1,0)$ and $(0,\pm1)$ plane waves through the $(\pm1,\pm1)$ grating vectors. This coupling lifts the degeneracy between the antisymmetric modes. Hence, for k_x=0, the

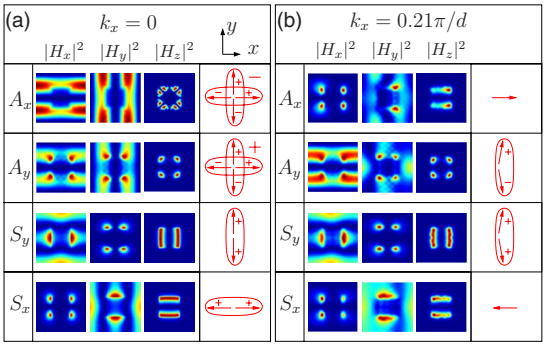

FIG. 3. (Color online) Magnetic field intensity of the four surface modes calculated with the Fourier modal method. (a) For $k_x=0$. (b) For $k_x=0.21\pi/d$. The field intensity is plotted on the interface ($z=0$) for a single period. High (respectively, low) intensity regions are shown in red (respectively, blue). Red arrows indicate the propagation direction of each single wave involved in surface modes, and the plus and minus signs show the symmetric and antisymmetric natures of the coupling.

modes A_x and A_y should not be described anymore as a standing wave resulting from the superposition of two counter-propagating surface waves, like in 1D structures, but rather as a standing wave resulting from the superposition of four surface waves (see Fig. 3). Such a coupling is allowed between the antisymmetric modes A_x and A_y, whereas it is forbidden for symmetry reasons between the symmetric modes S_x and S_y, which remain degenerate [see the blue curves in Fig. 2(a)].

Figure 3 shows the magnetic field intensities of the four surface modes calculated with the Fourier modal method for $k_x=0$ and $k_x=0.21\pi/d$. In Fig. 3(a), the distributions of the in-plane components of the magnetic field (H_x and H_y) evidence the symmetric and antisymmetric standing waves resulting from the coupling between two surface waves (S_x and S_y) and four surface waves (A_x and A_y). These coupled modes are schematically represented by the red arrows in Fig. 3(a), where the plus and minus signs represent the symmetric and antisymmetric natures of the coupling. In addition, the magnetic field z component H_z *a posteriori* validates the main approximation of the surface-impedance model, namely, the single TE mode approximation for the field in the hole. According to the magnetic field z component H_z, the hole modes are TE_{01}, TE_{10}, and TE_{11} for S_x, S_y, and A_y bands, respectively. However, for the A_x mode, the predominant waveguide mode in the apertures is a superposition of two antisymmetric hole modes, namely, TE_{11} and TE_{33}. This field calculation evidences why the surface-impedance model based on a single-mode approximation in the holes cannot predict the second band gap.

As soon as $k_x \neq 0$, the intricate four-waves mixing no longer holds. Figure 3(b) shows that the four surface modes can be accurately described with a single-mode approximation in the apertures and a one wave (S_x and A_x) or two-wave (S_y and A_y) picture above the metal. The slope of the A_x branch is not well predicted by the surface-impedance model in Fig. 2(a) since it has been calculated by using the antisymmetric TE_{11} hole mode. In fact, Fourier calculations show that as soon as $k_x > 0.2\pi/d$ the predominant mode in the holes is the symmetric one TE_{01} [see Fig. 3(b)]. We have checked that the asymptotic behavior of the A_x mode for large k_x values can be predicted by the model by using the TE_{01} hole mode in the dispersion matrix. The physical mechanism inducing this asymptote $d/\lambda \simeq 1.05$ is the proximity of the cut-off frequency of the TE_{01} mode, leading to a greater penetration depth into the apertures.

D. Free-space coupling

The magnetic field symmetries observed in Fig. 3 allow us to define the following selection rules for the external excitation of the surface modes by an incident plane wave, depending on its polarization. A TM-polarized incident plane wave with $k_y=0$ possesses a magnetic field oriented along the y axis and can only excite surface modes whose H_y components are symmetric with respect to the x axis; namely S_x, A_x, and A_y modes [solid curves in Fig. 2(a)]. Similarly, TE-polarized incident plane waves can only excite the S_y mode [dashed curve in Fig. 2(a)]. It is important to notice that the excitation of antisymmetric modes (A_x,A_y) vanishes at normal incidence due to symmetry reasons.

These selection rules include all surface modes supported by a two-dimensional perforated interface. They are important for the interpretation of the resonant features appearing in transmission and reflection spectra of metallic films textured with a two-dimensional array of subwavelength apertures. Let us emphasize that the selection rules derived from the model shed a different light on previous angle-resolved experimental[14] and theoretical[13] transmission spectra. In these works, the spectra were interpreted by using only two surface modes (S_x and A_x), like in 1D structures, instead of four. Actually, a careful analysis of Fig. 2(a) in Ref. 14 shows that the experiment indeed reveals three different bands, which can be associated to the excitation of S_x, A_x, and A_y modes by TM-polarized incident light. These three bands also appear in other recent angle-resolved experiments.[24] It is worth noticing that these selection rules remain valid in anisotropic plasmonic crystals ($d_x \neq d_y$).[25] In this case, the degeneracy between the symmetric modes S_x and S_y is lifted. If $d_x < d_y$, a coupling between the modes S_x and A_y occurs for nonzero wave vectors leading to a band gap between two coupled modes that can be described with a three-waves picture.[26] Although the model cannot predict the band-gap width, it can accurately predict the crossing position in the (ω,k) space as a function of all array parameters, including the aperture shape and size.

IV. INFLUENCE OF THE HOLE GEOMETRY

In this section, we take advantage of the analytical character of the model to derive simple trends for the dispersion relation of the surface mode with the lowest energy as a function of various geometrical parameters. In particular, we study the influence of the metal conductivity, the aperture area, and the aperture shape. Comparisons with experimental data further validate the model predictions and elucidate the origin of the fine resonance changes achieved by tuning the aperture shape.

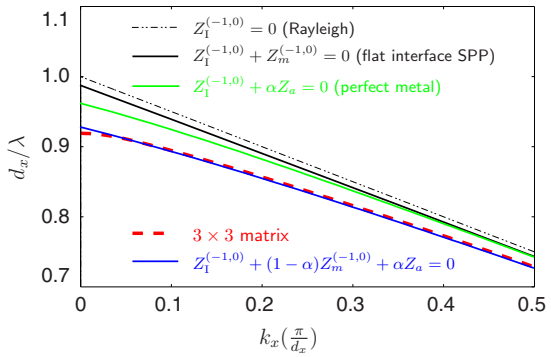

FIG. 4. (Color online) Surface mode S_x calculated with different degrees of approximation: analytical surface-impedance model with a 3×3 dispersion matrix (red dashed curve) and without coupling (blue curve), assuming perfect metal (green curve), assuming infinitely small holes (flat interface, solid dark curve), and Rayleigh anomaly (thin dark dashed line), which corresponds to the flat interface with perfect metal.

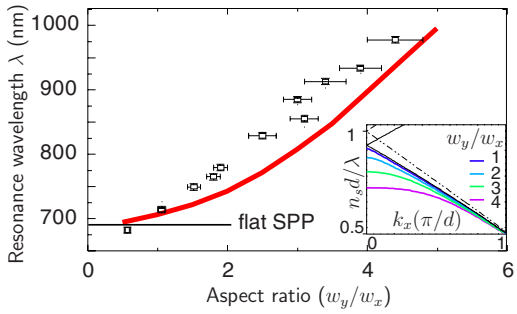

FIG. 5. (Color online) Influence of the aspect ratio w_x/w_y of rectangular holes on surface-plasmon resonances. The transmission resonance wavelengths measured through a drilled gold film are taken from Ref. 18 (black marks). They are compared with the position of the S_x mode calculated with the analytical model for $k_x=0$ (red curve). Horizontal dark line: SPP wavelength of the flat gold/substrate surface. Inset: dispersion curves of the fundamental S_x mode for four different aspect ratios.

A. Respective influence of the metal conductivity and the aperture area

In order to get further physical insight into the impact of the aperture size and shape on the surface modes, let us neglect the coupling between the different plane waves. According to the surface-impedance model, the dispersion relation of every folded branch (n,p) is then simply given by

$$Z_I^{(n,p)} + \alpha Z_a + (1-\alpha) Z_m^{(n,p)} = 0. \quad (15)$$

In Eq. (15), the influence of the hole shape and size is contained in the average surface impedance of the textured metal, which is simply driven by the propagation constant of the hole mode κ (through the hole impedance Z_a) and the apertures fill factor α.

Figure 4 shows the dispersion curve of the S_x surface mode calculated with different degrees of approximation. The influence of the coupling between counter-propagating surface waves is revealed by the comparison between the 3×3 matrix calculation (dashed red curves) and Eq. (15) (blue curve). It shows that the couplings induce a small redshift in the center of the first Brillouin zone, but they are negligible in the calculation of the real part of the surface mode frequency as soon as $k_x \neq 0$.

Additional approximations are now considered to clarify the influence of the apertures on surface modes. Considering infinitely small apertures $(\alpha \to 0)$ in Eq. (15) leads to the folded dispersion relation of the flat-interface SPP: $Z_I^{(-1,0)} + Z_m^{(-1,0)} = 0$ (dark curve in Fig. 4). Opening apertures in the smooth surface induces an increase in the average impedance because of the greater penetration depth in the apertures than in the metal $(|Z_a| > |Z_m^{(-1,0)}|)$. This average impedance increase results in a redshift of the dispersion curve for increasing hole widths. This is illustrated by the difference between the dark and blue curves in Fig. 4 (see also the hole width dependence of S_x, S_y, and A_y modes for $k_x=0$ in Figs. 2(b) and 2(c)]. This behavior predicted by the model and confirmed by Fourier calculations is in agreement with previous transmission experiments through drilled films.[15–17]

If perfect metal is considered $(Z_m^{(-1,0)}=0)$, the dispersion relation given by Eq. (15) leads to the "spoof surface-plasmon" model described in Refs. 8 and 9: $Z_I^{(-1,0)} + \alpha Z_a = 0$ (green curve). The difference between the green and blue curves demonstrates that the finite conductivity of the metal cannot be neglected. As a whole, Fig. 4 shows that the average surface impedance provides a mesoscopic description of surface modes on 2D metallic structures.

B. Influence of the aperture shape

In the last part, we focus on the model capability to predict fine resonance changes achieved by tuning the aperture shape. For this purpose, we compare the model predictions with transmission measurements carried out by van der Molen *et al.*[18] through gold films deposited on BK7 substrates (optical index n_s) and drilled with rectangular holes with a constant hole area ($\alpha=12\%$ and $d=425$ nm). Experiments have shown that the hole shape w_y/w_x strongly influences the resonance wavelength of the extraordinary transmission at normal incidence. This is illustrated in Fig. 5, where the wavelengths of the transmission peaks in Ref. 18 are shown as a function of the aspect ratio (black marks). At first sight, one may expect that the model would not predict this dispersive behavior obtained for constant α. Actually, this is not true. The red curve in Fig. 5 shows the model predictions for the S_x band at $k_x=0$ and for a gold permittivity given by a Drude model $\epsilon_m = 1 - \omega_p^2/(\omega^2 + i\omega\gamma)$, $\omega_p = 1.2 \times 10^{16}$ s^{-1} and $\gamma = 1.3 \times 10^{14}$ s^{-1}, and $n_s = 1.52$. Quantitative agreement with the experimental results is achieved; the slight difference being potentially attributed to an inevitable coupling for finite metal thicknesses of the BK7/gold surface mode with the air/gold surface mode in the experiment.[13] Referring to Eq. (15), the strong wavelength shift is understood as an enhancement of the hole impedance Z_a. Physically, this behavior is the consequence of an enhanced penetration depth into the rectangular apertures, due to a decrease in the cut-off frequency of the fundamental TE_{01} hole mode as w_y/w_x increases.[21] As one approaches the cut-off, the surface mode is more and more governed by the hole

mode. The cut-off frequency decrease for large aspect ratios does not only induce a redshift of the surface mode energy for $k_x=0$ but also a strong flattening of the entire S_x band, as evidenced in the inset of Fig. 5.

V. CONCLUSION

In summary, we have derived closed-form expressions for the dispersion relation of surface modes supported by metallic surfaces perforated by 2D arrays of subwavelength apertures. The model predictions that take into account the radiative and nonradiative damping of the mode are in quantitative agreement with fully vectorial Fourier calculations and with recent experimental results. Vectorial calculations have shown that the biperiodicity induces an unexpected coupling between orthogonal SPP waves that leads to a double plasmonic band gap in the center of the first Brillouin zone. The model sheds a different light on previous experiments and clarifies the impact on the surface modes of a number of geometrical and material parameters such as the aperture shape and size or the metal conductivity. Indeed, the model evidences that the surface mode of a textured interface can be mainly described by the dispersion relation of a flat interface provided that the metal be replaced by an average metallic medium whose effective properties depend on the optogeometrical parameters of the surface [see Eq. (15)]. The formalism described in this paper is then very simple and provides an efficient tool for further engineering of plasmonic devices and metallic metamaterials.

ACKNOWLEDGMENTS

The authors would like to thank Jean-Paul Hugonin for the help. We acknowledge financial support from the European Network of Excellence NEMO.

*stephane.collin@lpn.cnrs.fr

[1] S. M. Rytov, Sov. Phys. JETP **2**, 466 (1956).
[2] E. Yablonovitch, Phys. Rev. Lett. **58**, 2059 (1987).
[3] V. M. Shalaev, Nat. Photonics **1**, 41 (2007).
[4] *Surface Plasmons*, edited by H. Raether (Springer, Berlin, 1988).
[5] T. W. Ebbesen, H. J. Lezec, H. F. Ghaemi, T. Thio, and P. A. Wolff, Nature (London) **391**, 667 (1998).
[6] C. Genet and T. W. Ebbesen, Nature (London) **445**, 39 (2007).
[7] R. Ulrich and M. Tacke, Appl. Phys. Lett. **22**, 251 (1973).
[8] J. B. Pendry, L. Martín-Moreno, and F. J. Garcia-Vidal, Science **305**, 847 (2004).
[9] F. J. Garcia-Vidal, L. Martín-Moreno, and J. B. Pendry, J. Opt. A, Pure Appl. Opt. **7**, S97 (2005).
[10] H. Liu and P. Lalanne, Nature (London) **452**, 728 (2008).
[11] F. J. García de Abajo and J. J. Sáenz, Phys. Rev. Lett. **95**, 233901 (2005).
[12] L. Martín-Moreno and F. J. García-Vidal, J. Phys.: Condens. Matter **20**, 304214 (2008).
[13] P. Lalanne, J. C. Rodier, and J. P. Hugonin, J. Opt. A, Pure Appl. Opt. **7**, 422 (2005).
[14] W. L. Barnes, W. A. Murray, J. Dintinger, E. Devaux, and T. W. Ebbesen, Phys. Rev. Lett. **92**, 107401 (2004).
[15] K. L. van der Molen, F. B. Segerink, N. F. van Hulst, and L. Kuipers, Appl. Phys. Lett. **85**, 4316 (2004).
[16] K. J. Klein Koerkamp, S. Enoch, F. B. Segerink, N. F. van Hulst, and L. Kuipers, Phys. Rev. Lett. **92**, 183901 (2004).
[17] A. Degiron and T. W. Ebbesen, J. Opt. A, Pure Appl. Opt. **7**, S90 (2005).
[18] K. L. van der Molen, K. J. Klein Koerkamp, S. Enoch, F. B. Segerink, N. F. van Hulst, and L. Kuipers, Phys. Rev. B **72**, 045421 (2005).
[19] J. D. Jackson, *Classical Electrodynamics* (Wiley, New York, 1999).
[20] A. Yariv and P. Yeh, *Classical Electrodynamics* (Wiley, New York, 1984).
[21] S. Collin, F. Pardo, and J.-L. Pelouard, Opt. Express **15**, 4310 (2007).
[22] *Handbook of Optical Constants of Solids*, edited by E. D. Palik (Academic, Orlando, 1985).
[23] W. L. Barnes, T. W. Preist, S. C. Kitson, and J. R. Sambles, Phys. Rev. B **54**, 6227 (1996).
[24] M.-W. Tsai, T.-H. Chuang, H.-Y. Chang, and S.-C. Lee, Appl. Phys. Lett. **88**, 213112 (2006).
[25] C. Billaudeau, S. Collin, C. Sauvan, N. Bardou, F. Pardo, and J.-L. Pelouard, Opt. Lett. **33**, 165 (2008).
[26] C. Sauvan, C. Billaudeau, S. Collin, N. Bardou, F. Pardo, J.-L. Pelouard, and P. Lalanne, Appl. Phys. Lett. **92**, 011125 (2008).